Novel Dynamic Voltage Support Capability of Photovoltaic Systems for Improvement of Short-Term Voltage Stability in Power Systems

K. Kawabe, *Member, IEEE*, Y. Ota, *Member, IEEE*, A. Yokoyama, *Member, IEEE*, and K. Tanaka

Abstract—The large integration of photovoltaic (PV) power generation systems into power systems causes deterioration in power system stability. In our previous work, we showed that reactive power control using the inverters of PV systems, known as dynamic voltage support (DVS) capability, is a promising approach to improve the short-term voltage stability in power systems. In the present paper, we propose a novel DVS capability as a function of PV inverters. In contrast to the conventional DVS capability, the proposed method uses both active and reactive power injection to improve the short-term voltage stability. Numerical examples show that the proposed DVS capability further improves the short-term voltage stability compared with the conventional DVS capability. Further, the proposed method can alleviate a frequency drop after a fault caused by interruption in PV systems.

Index Terms—Fault-induced delayed voltage recovery, fault ride-through capability, induction motors, photovoltaic power generation, reactive power control, short-term voltage stability, transient stability.

NOMENCLATURE

E	voltage behind the electric filter of a photovoltaic (PV) system
V	voltage at a PV-connected bus
X	reactance of the electric filter of a PV system
P_{PV}	active power output of a PV system
Q_{PV}	reactive power output of a PV system
P_{ref}	reference value of active power output of a PV system
Q_{ref}	reference value of reactive power output of a PV system
I	current output of a PV system
I_{max}	current rating of a PV inverter
K_P	gain constant of an automatic power regulator (APR)
T_P	time constant of an APR
K_C	gain constant of an automatic current regulator (ACR)
T_C	time constant of an ACR
$P_{ref,pre}$	P_{ref} before voltage sag
$Q_{ref,pre}$	Q_{ref} before voltage sag
V_{pre}	voltage at a PV-connected bus before voltage sag
t	time
t_{cl}	fault clearing time
σ_d	sensitivity coefficient of the terminal voltage of a PV system with respect to the active current output
σ_q	sensitivity coefficient of the terminal voltage of a PV system with respect to the reactive current output
α	positive constant
ω	rotor speed of an induction motor load

I. INTRODUCTION

THE installation of renewable energy sources (RESs) is a recent social trend toward the development of sustainable electric power systems. Policies, e.g., feed-in tariff (FIT) scheme, have increased the installed capacity of RESs in many countries. In Japan, the capacity of solar PV systems to be installed has drastically increased since the government introduced the FIT scheme in 2012.

On the other hand, researchers have shown that the large penetration of PV systems can affect power system stability. Short-term voltage stability is one of the issues of concern in the transient region after a disturbance in a power system [1]. In our previous work, we have shown that the sudden interruption of PV systems after a disturbance can deteriorate the short-term voltage stability [2].

Short-term voltage instability occurs for a few seconds. The basic mechanism of the short-term voltage stability caused by the dynamic characteristics of induction motor (IM) loads was presented several decades ago in [3] and [4]. Although short-term voltage instability is less well known compared with rotor-angle instability, many works have studied load modeling and methods to analyze the short-term voltage stability [5]-[8]. In recent years, the importance of load modeling to analyze fault-induced delayed voltage recovery,

which is closely related to the short-term voltage stability, has been renewed and investigated as reported in [9] and [10]. Considering that a large number of PV systems are being installed near load centers, developing countermeasures to avoid short-term voltage instability caused by sudden interruption in PV systems is important.

The injection of reactive power by PV systems is a promising approach to prevent deterioration in the short-term voltage stability. This function is known as dynamic voltage support (DVS) capability. Dynamic simulations at the transmission and distribution network levels have also been carried out in several studies to verify the effectiveness of the DVS capability on the short-term voltage stability [2], [11]-[15].

In the present paper, we propose a novel DVS capability as a function of the PV system to improve the short-term voltage stability. Section II describes the modeling of PV systems used for the transient analysis. The PV model can consider the control system of an inverter, fault ride-through (FRT), and DVS capability. Section III explains the control action expected from the proposed DVS capability and how to achieve this control action in the control system of the PV inverter. In contrast to the conventional DVS capability, the proposed DVS capability injects both reactive and active power using the PV system while maintaining the rated current capacity of the inverter. Numerical examples are presented in Sections IV and V for a one-load infinite-bus (OLIB) system and a multimachine power system, respectively, to compare the effects of the proposed DVS capability on the short-term voltage stability with those of the conventional one.

II. MODELING OF PV SYSTEMS

A. Equivalent Circuit

Fig. 1 shows the equivalent circuit of the PV model for the transient analysis. The PV model consists of a voltage source and reactance of an electric filter. Here, X is set to 0.07 p.u. using the machine rating as the base. In the model, we consider the control system of the inverter to cover a simulation time frame of several seconds in duration with integration time steps of 1 ms. The dynamics of the DC side of the inverter is neglected because the time delay for the control systems in the DC side is sufficiently small compared with the integration time step in general. Internal voltage $\vec{E}$ is varied according to the control system of the inverter, as described below. The fundamental configuration of the model is similar to that of the model developed in [16].

B. Control System of the Inverter

The control system of the inverter consists of an automatic power regulator (APR) and an automatic current regulator (ACR), as shown in Fig. 2. Subscript d represents the d axis corresponding to the phase angle of bus voltage $\vec{V}$. Subscript q represents the q axis, which lags behind the d axis by 90°.

Table I lists the gain and time constants of the control system that are tuned so that the system is stable in the following numerical examples in terms of the small-signal stability.

The output of the PV system is assumed to be limited by rated current I_{max}. In the APR, we need to determine the reference values of active current $I_{d,ref}$ and reactive current $I_{q,ref}$ in a coordinated manner to maintain the current output within I_{max}. When we model a PV system that does not have a DVS capability, we prioritize the active current in the current-limiting process by following the control flow shown by the dotted line in Fig. 2 and setting $I_{d,max}$ and $I_{q,max}$ to

$$I_{d,\max} = I_{\max}, \quad I_{q,\max} = \sqrt{I_{\max}^2 - I_{d,ref}^2}. \quad (1)$$

On the other hand, we apply different current allocation logic
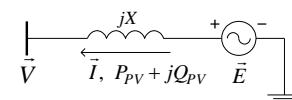
Fig. 1. Equivalent circuit of the PV model.
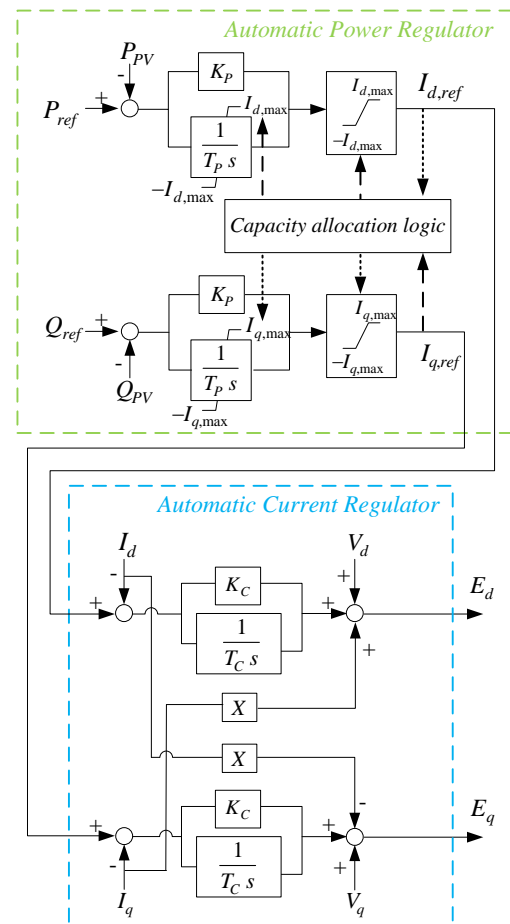
Fig. 2. Control system of the PV inverter.

TABLE I
CONTROL PARAMETERS IN THE CONTROL SYSTEM OF A PV INVERTER

K_P	T_P (s)	K_C	T_C (s)
0.10	0.05	0.10	0.10

when we apply the conventional or proposed DVS capability, as described later. The allocation logic is an important issue in this study, which will be described in Section III.

C. FRT Capability

FRT capability is a grid interconnection requirement of the PV system to prevent a cascading frequency drop. New FRT requirements have been proposed in Japan through a Japanese governmental research project [17]; they were introduced in the grid code in 2014. During a voltage sag, the PV inverters are not required to shut off. Even if the operation of the PV system is interrupted, recovering the output of the PV system as soon as possible is preferable to prevent variations in the power system frequency.

In this study, the FRT capability is indicated by setting threshold voltage V_{LVRT} for the voltage sag and recovery speed T_{FRT} of the output after a fault is cleared. The operation of the PV model stops if the terminal voltage is less than V_{LVRT} per unit. When the operation stops, the active power output recovers up to 80% of that before the fault within T_{FRT} seconds after a voltage recovery [2]. The active power recovery is modeled by changing P_{ref} in the APR in Fig. 2 according to

$$P_{ref}(t) = \begin{cases} P_{ref,pre} \times (t - t_{cl})/\tau & (P_{ref}(t) \le P_{ref,pre}) \\ P_{ref,pre} & (P_{ref}(t) > P_{ref,pre}) \end{cases}, \quad (2)$$

where $P_{ref,pre}$ is the active power output before the fault. Time constant τ is set to satisfy an assumed T_{FRT}. Delay in the active power recovery indicates a delay in the maximum power point tracking by a DC–DC converter after a voltage sag, although the control system of the DC–DC converter is not modeled in detail. We note that a change in the active power caused by a sudden change in the weather is neglected in this study because we focus on the stability problem in the transient period.

In this study, V_{LVRT} is set to 0.2 p.u. and T_{FRT} is set to 0.2 s for the PV systems with FRT capability. These values have been selected according to the technical targets recommended in the newly proposed Japanese requirements for PV systems connected after 2016 [17].

D. DVS Capability

In this study, the DVS capability is modeled by changing Q_{ref} in the APR according to

$$Q_{ref}(t) = Q_{ref,pre} + K_{DVS} \times I_{max} \times (V_{pre} - V(t)), \quad (3)$$

where K_{DVS} determines the rate of change in the reactive power with respect to the change in the terminal voltage. In this study, $K_{DVS} = 5$ to output a maximum reactive current when the voltage deviation is 0.2 p.u. The reactive power before voltage sag $Q_{ref,pre}$ is set to zero in this study under the assumption that every PV system operates at a unity power factor in the normal state. The voltage at a PV-connected bus before voltage sag V_{pre} can be available by logging the terminal voltage at a constant frequency and using the voltage when the PV system detects the voltage sag. In a real

implementation, dead band should be set so that the DVS capability is not triggered in the normal state.

In the current allocation logic in the APR, we prioritize the reactive current in the current limiter by following the control flow shown by the dashed line in Fig. 2 and setting $I_{d,max}$ and $I_{q,max}$ to

$$I_{d,max} = \sqrt{I_{max}^2 - I_{q,ref}^2}, \quad I_{q,max} = I_{max}. \quad (4)$$

III. PROPOSED DVS CAPABILITY

A. Concept of the Proposed DVS Capability

A PV system with conventional DVS capability injects reactive current up to the rated capacity when the terminal voltage is sufficiently low, whereas it limits the active current down to zero because of the capacity allocation logic in the APR, as described in Section II-D. The prioritized reactive current injection improves the short-term voltage stability, as discussed in [2].

Although little doubt exists that the prioritized reactive current injection is effective for the increase in the terminal voltage, allocation of the entire current capacity to the reactive current does not mean that it maximizes the voltage increase. Assuming that sensitivity coefficients σ_d and σ_q of the terminal voltage of the PV system with respect to the active- and reactive-current outputs are respectively defined as

$$\sigma_d = \partial V / \partial I_d \quad , \quad \sigma_q = \partial V / \partial I_q \,, \quad (5)$$

the change in the terminal voltage with respect to the injections of I_d and I_q can be approximately expressed by

$$\Delta V \cong \sigma_d I_d + \sigma_q I_q. \quad (6)$$

Then, we can formulate the following optimization problem for the maximization of the terminal voltage through the active- and reactive-current injection by the PV system:

$$\textit{Maximize} \qquad f = \Delta V = \sigma_d I_d + \sigma_q I_q \qquad (7)$$

$$\textit{Subject to} \qquad I_d^2 + I_q^2 = I_{max}^2 \,, \qquad (8)$$

$$0 \le I_d \,, \ 0 \le I_q \,. \qquad (9)$$

Obviously, the injection of reactive current only is not the optimal solution to maximize the voltage increase considering the above optimization problem. By assuming that we know the sensitivity coefficients, we can possibly determine the active and reactive currents that maximize the terminal voltage. However, calculating the sensitivity coefficients using only local information is difficult.

In this paper, we propose to output active and reactive currents to support the terminal voltage as follows:

$$I_d = I_q = I_{max} / \sqrt{2} \,, \qquad (10)$$

For the output in (10), the objective function in (7) is calculated as

$$f_{pro} = \frac{(\sigma_d + \sigma_q)}{\sqrt{2}} I_{max} . \qquad (11)$$

On the other hand, if we inject a reactive current at the rated capacity, the objective function in (7) is calculated as

$$f_{con} = \sigma_q I_{max} . \qquad (12)$$

By defining $\sigma_d = K$ and $\sigma_q = \alpha K$, the condition for $f_{pro} > f_{con}$ is calculated as

$$\alpha < 1 + \sqrt{2} \cong 2.41 . \qquad (13)$$

In other words, the proposed active- and reactive-power injection in (10) increases the terminal voltage more than the reactive power injection by the conventional DVS capability despite the connected voltage level if the difference in the sensitivity satisfies (13). Although the magnitude of α is different depending on the location of the PV system and the system configuration and varies from moment to moment, it is empirically expected to satisfy (13). In this paper, we will demonstrate in the following numerical examples that the active- and reactive-current injection in (10) improves the short-term voltage stability more than the conventional DVS capability even though α is unknown.

B. Control System for the Proposed DVS Capability

To realize the proposed DVS capability, we change Q_{ref} according to (3) and apply an original current allocation logic to the APR in the control system of the PV inverter. The proposed control system follows the control flow indicated by the dashed line in Fig. 2 and sets $I_{d,max}$ and $I_{q,max}$ to

$$I_{d,max} = \sqrt{I_{max}^2 - I_{q,ref}^2}, \quad I_{q,max} = I_{max}/\sqrt{2} . \quad (14)$$

IV. NUMERICAL EXAMPLES OF AN OLIB SYSTEM

A. Test System and Comparative Cases

The OLIB system shown in Fig. 3 is used to focus on the short-term voltage stability. An extra-high voltage (EHV) network is modeled using an infinite bus, and the dynamic characteristics of the generators are neglected. The load center is represented by a dynamic load connected through aggregated transmission and subtransmission lines. Although the impedance of low voltage feeders also needs to be considered for more quantitative analysis, they are neglected in this study. The dynamic load consists of a first-order IM
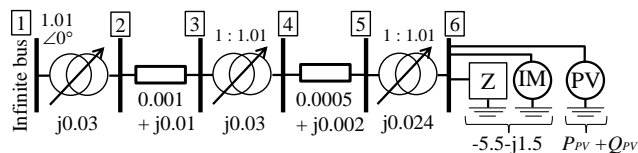
Fig. 3. OLIB system.

and a constant impedance (Z), as shown in Fig. 3. The ratio of IM to the total load is set to 50%. Here, we assume a relatively high IM load ratio to focus on the short-term voltage stability.

The aggregated PV system is connected to the load bus. The active power output of the PV system is 3.0 p.u., which corresponds to 60% of the total load, and it operates at a unity power factor in the normal state. The rated current capacity of the PV system is set to 3.3 p.u. Although we consider only the aggregated PV system connected to the load center to prevent a complicated discussion of the result, some PV systems in actual grids would be connected far from the load centers.

Three simulation cases are compared to study the effects of the proposed DVS capability on the short-term voltage stability. Case I is the base case in which the PV system does not have a DVS capability. On the other hand, we assume PV systems with conventional and proposed DVS capabilities for Cases II and III, respectively. The dynamic simulations are carried out under two fault scenarios described in the next sections.

B. Results for Fault Scenario A

In fault scenario A, a three-line-to-ground (3LG) fault in the EHV network is assumed by setting the voltage of Bus 1 to 0.1 p.u. The PV system temporarily stops immediately after the fault because the voltage at Bus 6 falls below the threshold value of 0.2 p.u. in the FRT capability. The dynamic characteristics after fault clearing are different among the three cases.

Table II lists the critical clearing times (CCTs) when the IM stalls under fault scenario A. As observed from the comparison, equipping the PV system with DVS capability improves the short-term voltage stability even if the PV system is temporarily shut off due to the fault. It also shows that the proposed DVS capability is more effective than the conventional one.

Fig. 4 compares the change in the voltage at Bus 6 when we set fault duration time t_{cl} to 0.16 s. The DVS capability avoids voltage collapse in Cases II and III. We also observe that the proposed DVS capability speeds up the voltage recovery in Case III compared with that in Case II.

Fig. 5 shows the comparison of the output of the PV system for Cases II and III when $t_{cl} = 0.16$ s. In Case II, the PV system injects reactive current at the rated current capacity immediately after fault clearing. Then, the reactive current decreases with the increase in the terminal voltage, whereas the active current increases. On the other hand, in Case III, the proposed DVS capability injects both active and reactive currents immediately after fault clearing while maintaining the current capacity. With the voltage recovery, the PV system reverts to the active power output and decreases the reactive current.

To compare the effects of the conventional and proposed DVS capabilities on the short-term voltage stability, we show the change in the operating point of the load in the $P{-}V$ plane for Cases II and III in Fig. 6 when $t_{cl} = 0.16$ s. Here, P and V

represent the active power consumption and the magnitude of the terminal voltage of the load, respectively. We also describe the transient *P–V* curve [18] that indicates the power transmission capability to the load at $t = 0.50$ s when the PV system injects maximum current. The transient *P–V* curve can be depicted for a given time step during the transient period by changing the rotation speed ω of the IM load over the entire operating range $0 \leq \omega \leq 1$, which is independent of the time-domain simulation.

From the comparison of the transient *P–V* curves shown in Fig. 6, we can observe that the simultaneous active- and reactive-power injection by the proposed DVS capability at $t = 0.50$ s further enhances the transmission capability to the load compared with the reactive power injection by the conventional DVS capability. As a result, the operating point of the load in Case III moves along the locus where power

consumption is larger than that in Case II. Therefore, the re-acceleration of the IM load after fault clearing in Case III is larger than that in Case II, which shows how the proposed DVS capability further improves the short-term voltage stability.

C. Results for Fault Scenario B

In fault scenario B, a 3LG fault located far from the load center in the EHV network is simulated by setting the voltage of Bus 1 to 0.6 p.u. The PV system does not stop operating under this scenario.

The CCTs for fault scenario B are listed in Table III. The comparison shows that the proposed DVS capability can improve the short-term voltage stability for a shallow voltage sag as well as in fault scenario A. A voltage collapse does not occur in Case III at any of the fault duration time, and the reason is discussed below.

Fig. 7 shows the comparison of the voltage at Bus 6 among the three cases when $t_{cl} = 0.4$ s. A voltage collapse occurs in Case I due to stalling of the IM load. On the other hand, the voltage recovers after fault clearing in Cases II and III. The results show that the application of the proposed DVS capability is the most effective for the voltage increase even during a 3LG fault.

In Case II, the PV system with the conventional DVS capability injects reactive power after the fault, whereas it decreases the active power down to zero, as shown in Fig. 8(a). On the other hand, in Case III, the PV system decreases the

TABLE II
CCTs FOR FAULT SCENARIO A

Case I	Case II	Case III
0.128	0.229	0.262
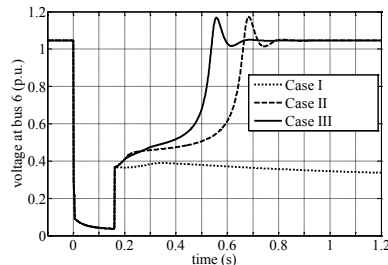
Fig. 4. Change in the voltage at Bus 6 under fault A.
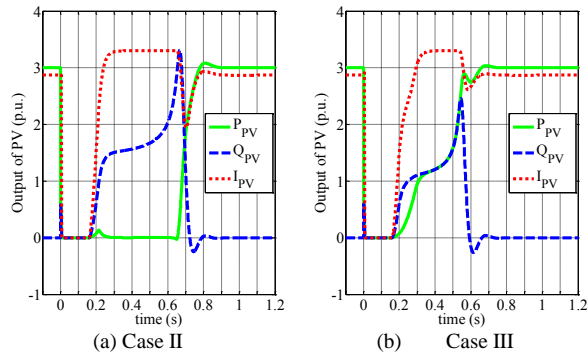
(a) Case II   (b)   Case III

Fig. 5. Power and current outputs of the PV system under fault A.
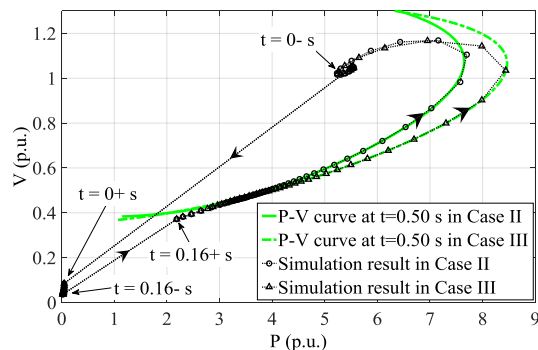
Fig. 6. Discussion in the *P–V* plane under fault A.

TABLE III
CCTs FOR FAULT SCENARIO B

Case I	Case II	Case III
0.370	0.702	∞
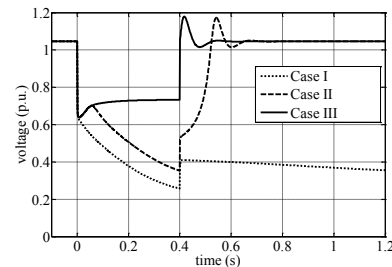
Fig. 7. Change in the voltage at Bus 6 under fault B.

(a) Case II   (b)   Case III
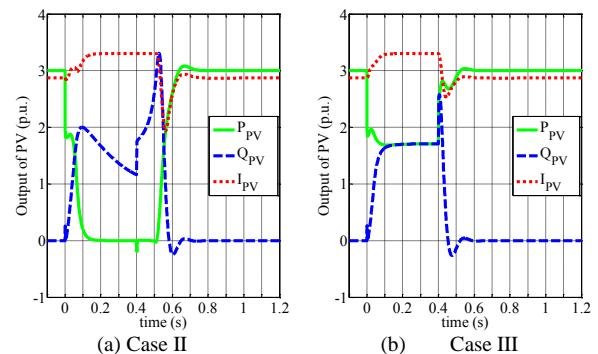
Fig. 8. Power and current outputs of the PV system under fault B.

active power output to $I_{max}/\sqrt{2}$ and injects the same amount of reactive power, as shown in Fig. 8(b), by applying the proposed current allocation logic.

Fig. 9 shows the change in the operating point of the load in the $P–V$ plane for Cases II and III when $t_{cl} = 0.4$ s. In addition to the operating point, we describe the change in the transient $P–V$ curve during the fault. We also show the stability boundary line [8] for the IM load. Assuming that the rotor speed that achieves maximum value of the conductance is defined as ω_t, the operating range of the load in the $P–V$ plane is above the load characteristic curve at $\omega = \omega_t$ [8]. The stability boundary divides the region above the load characteristic curve into two regions in which the IM load accelerates and decelerates. The overview of the analytical method is explained in [8].

In Case II, the transient $P–V$ curve expands from $t = 0 + $ s to $t = 0.06$ s and settles after $t = 0.2$ s, as shown in Fig. 9(a). From $t = 0.2$ s to $t = 0.4 − $ s, the load operating point moves downward along the transient $P–V$ curve because the transient $P–V$ curve exists in the deceleration region. After fault clearing, the operating point jumps to the upper right and moves upward because the operating point lies in the acceleration region.

In Case III, the transient $P–V$ curve expands from $t = 0 + $ s to $t = 0.2$ s and settles after $t = 0.2$ s, as shown in Fig. 9(b). From the comparison of the transient $P–V$ curves from $t = 0.2$ s to $t = 0.4 − $ s between Cases II and III, the simultaneous active- and reactive-power injection in Case III further enhances the transient $P–V$ curve compared with the reactive
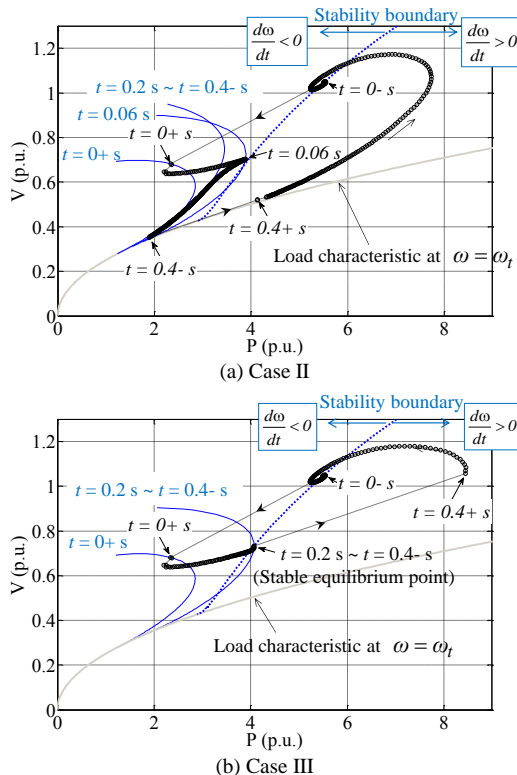
power injection in Case II. Because a stable equilibrium point (SEP) exists at the intersection of the stability boundary of the transient $P–V$ curve from $t = 0.2$ s to $t = 0.4 − $ s, the operating point settles at the SEP during the 3LG fault. Therefore, a voltage collapse does not occur in Case III in any of the fault duration time.

V. NUMERICAL EXAMPLES OF A MULTIMACHINE POWER SYSTEM

A. Test System and Comparative Cases

The effectiveness of the proposed DVS capability is verified for a modified 10-machine New England power system shown in Fig. 10. In Fig. 10, we show the active power output of the generators and the active power consumption of the loads according to the per unit values on a 100-MVA base. The total demand is set to 4262 MW. The reference frequency is 60 Hz. The generators are modeled using a classical model, and the governor of the first-order model is incorporated into each generator. Generator G1 at bus 39 is modeled as a swing generator.

The modified test system contains 18 load centers. To focus on the short-term voltage stability, we model every load except L18 at bus 39 as the dynamic load used in the previous section, and we consider a feeder equivalent [10] using an aggregated subtransmission system (whose configuration is the same as that shown in Fig. 3), as shown in the example in Fig. 10. The impedance shown in Fig. 3 is converted for each subtransmission system by considering the power consumption of each load center. The load center at bus 39 is modeled by a constant impedance.

The PV systems are connected to the load centers, except L5 and L18. All PV systems operate at a unity factor, and the active power output of each PV system is 30% of each load center. The rated current capacity of each PV system is set to

Fig. 9. Discussion in the $P−V$ plane under fault B.
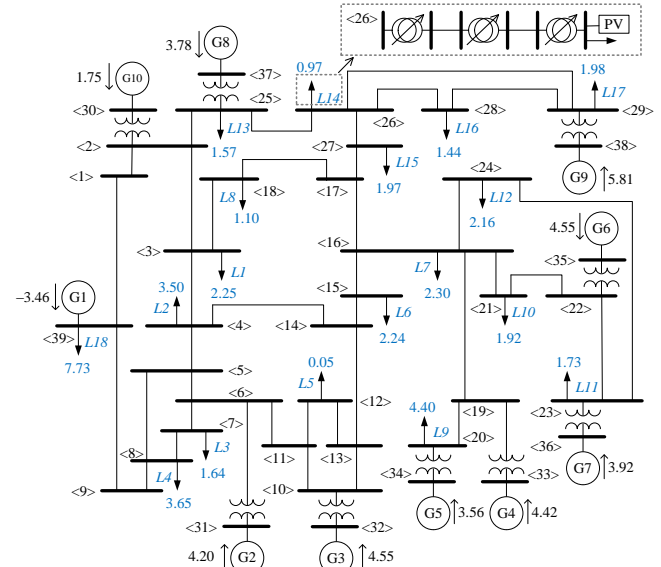
Fig. 10. Modified 10-machine New England power system.
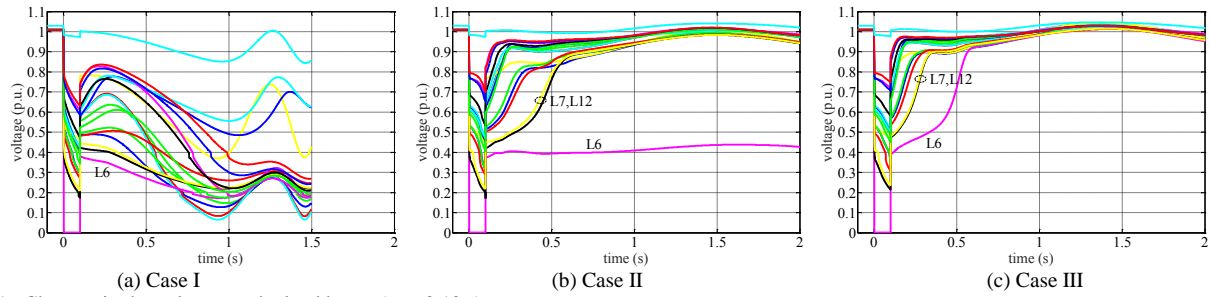
Fig. 11. Changes in the voltages at the load buses (t_{cl} = 0.10 s).

(a) Case I   (b) Case II   (c) Case III
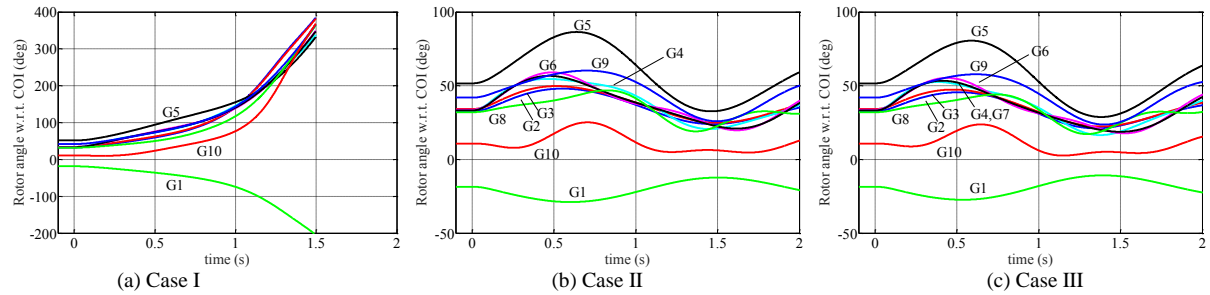
Fig. 12. Changes in the rotor angles with respect to the center of inertia (COI) (t_{cl} = 0.10 s).

(a) Case I   (b) Case II   (c) Case III

TABLE IV
CCTs UNDER 3LG FAULTS IN THE MODIFIED 39-BUS SYSTEM

Fault Location	Case I (s)	Case II (s)	Case III (s)
2-3	0.093	0.129	0.152
3-18	0.075	0.097	0.120
15-16	0.079	0.107	0.124
17-18	0.069	0.084	0.098
18-17	0.083	0.108	0.128
24-16	0.077	0.096	0.112

TABLE V
LOAD CENTERS WHERE THE PV SYSTEMS ARE SHUT OFF DURING FAULT
"15–16" FOR 0.1 S

	Load center where 100% of the PV systems are shut off	Load centers where 50% of the PV systems are shut off
Case I	L6, L7	L1, L2, L8, L10, L12, L15
Case II	L6, L7	L2, L8, L10, L12
Case III	L6	L2, L7, L8, L10, L12

1.1 times the active power output at the per unit value.

We assume that the FRT capability does not work well for 50% of the PV systems installed at each load center. These PV systems are modeled by setting V_{LVRT} to 0.4 p.u. and T_{FRT} to ∞ s. Therefore, the PV systems stop operating if the terminal voltage falls below 0.4 p.u. and never restart during the simulation. For the other 50% of the PV systems at each load center, we assume the following three types. In Case I, the systems have only the FRT capability. In Cases II and III, they have the conventional and proposed DVS capabilities, respectively.

B. Improvement of Short-Term Voltage Stability

Table IV lists the comparison of the CCTs under 3LG faults at various locations. The CCT is used as an index for the short-term voltage stability because a voltage collapse occurs when the power system is unstable. The notation "*n–m*" represents a 3LG fault that occurs near bus *n* and is cleared by opening one circuit in the line *n–m*. As listed in Table IV, the CCTs improve because of the application of the DVS capability. Moreover, we confirm from the comparison between Cases II and III that the proposed DVS capability is more effective than the conventional one to improve the short-term voltage stability.

Figs. 12 and 13 show the comparison of the results between the cases under fault "15–16" when the fault duration time is set to 0.1 s. In Case I, a voltage collapse occurs around L6, which is near the fault location, as shown in Fig. 11(a). The voltage collapse causes the stepping out of the generators, as shown in Fig. 12(a). In Case II, the application of the conventional DVS capability to some of the PV systems prevents a large-scale voltage collapse. However, a local voltage collapse occurs at L6. The voltage instability phenomenon is stabilized when we apply the proposed DVS capability in Case III.

Table V lists the summary of the load centers where the PV systems are shut off during fault "15–16" when the fault duration time is set to 0.1 s. From the results, all PV systems at L7 are shut off in Cases I and II because the terminal voltage falls below 0.2 p.u. during the fault. On the other hand, half of the PV systems at L7 continue operating in Case III owing to the better voltage support of the proposed DVS capability. Around the fault location, the terminal voltage falls below 0.4 p.u., and 50% of the PV systems where the FRT capability does not work well are shut off and never restarted.

We note that we have not investigated the effect of the proposed DVS capability on the transient stability in this work. In the numerical examples with high IM load ratio, we clearly show that the higher ability of the PV systems to support the voltage contributes to the improvement in transient stability.

(a) Case II   (b) Case III
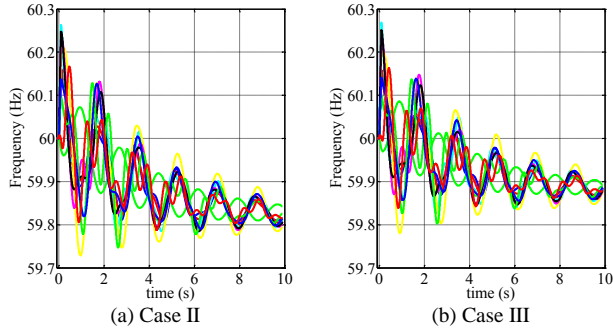
Fig. 13. Change in the frequencies ($t_{cl} = 0.09$ s).

(a) Case II   (b) Case III
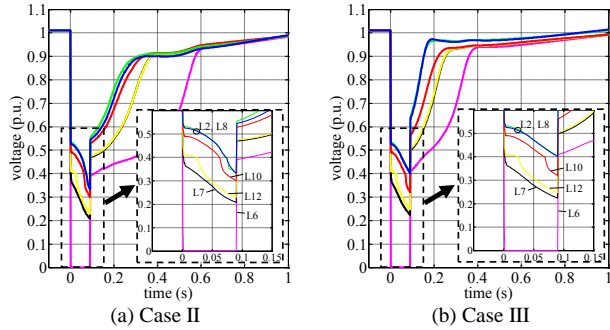
Fig. 14. Change in the voltages at the load buses ($t_{cl} = 0.09$ s).

TABLE VI
LOAD CENTERS WHERE THE PV SYSTEMS ARE SHUT OFF DURING FAULT
"15–16" FOR 0.09 S

	Load center where 100% of the PV systems are shut off	Load centers where 50% of the PV systems are shut off
Case II	L6	L2, L7, L8, L10, L12
Case III	L6	L7, L10, L12

However, further study would be required to investigate its effect on the transient stability under other load-modeling conditions, e.g., when the ratio of the IM load to the total load is low.

C. Effect on the Frequency Stability

The application of the proposed DVS capability also positively affects the short-term frequency stability. Fig. 13 shows the comparison of the changes in the frequencies between Cases II and III under fault "15–16." Here, we set the fault duration time to 0.09 s to observe the stable cases in terms of the short-term voltage and transient stability.

Fig. 13 shows that the frequencies of the synchronous generators decrease in both cases. We also observe that the application of the proposed DVS capability in Case III alleviates the frequency decrease compared with the results in Case II because the number of PV systems that are shut off after the fault is different between Cases II and III, as listed in Table VI. The PV systems at L2 and L8 continue operating in Case III, whereas they stop in Case II.

Fig. 14 shows the comparison of the voltages at the load buses listed in Table VI. The voltages at L2 and L8 fall below 0.4 p.u. in Case II, whereas the voltages are supported above 0.4 p.u. in Case III because the effect of the proposed DVS

capability on the voltage increase is higher than that of the conventional one.

VI. CONCLUSION

In this paper, we have proposed a novel DVS capability of PV systems to improve the short-term voltage stability. The proposed DVS capability injects active and reactive power in a coordinated manner as a function of the terminal voltage. The numerical examples have demonstrated the greater effectiveness of the proposed method for improving the short-term voltage stability compared with the conventional DVS capability. We have also shown that the application of the proposed method can help alleviate the frequency drop after a fault because better voltage support can reduce the number of PV systems that are shut off due to a voltage sag.

In our future works, the applicability of the proposed method will be verified by field tests that consider other important conditions such as unbalanced faults and protection systems. In addition, we will verify the effectiveness of the proposed method for transient stability in a test system with a lower IM load ratio because we assumed a high IM load ratio in this study to focus on the short-term voltage stability. Coordination with other controllable equipment such as flexible alternating current transmission system and battery energy storage devices is also an important issue for the integration of RESs while maintaining power system stability.

APPENDIX

For an additional explanation on the different rate of active current output to the entire current capacity of the PV system described in Section III-A, we derive the relationship between α and the rate of active current injection of the PV system.

Assuming that the PV system injects active- and reactive-current as

$$I_d = \beta I_{max}, \quad I_q = \sqrt{1 - \beta^2} I_{max}, \quad (0 \le \beta \le 1), \quad (15)$$

the objective function in (7) is calculated as

$$f_{app} = \sigma_d \beta I_{max} + \sigma_q \sqrt{1 - \beta^2} I_{max}. \quad (16)$$

By defining $\sigma_d = K$ and $\sigma_q = \alpha K$, the condition for $f_{app} > f_{con}$ is calculated as

$$\beta < \frac{2\alpha}{1 + \alpha^2}. \quad (17)$$

Although α differs depending on the location of the PV system and varies from moment to moment, the active- and reactive-current injection in (15) increases the terminal voltage more than the reactive current injection by the conventional DVS capability if coefficient β satisfies (17).

REFERENCES

[1] P. Kundur, J. Paserba, V. Ajjarapu, G. Andersson, A. Bose, C. Canizares, N. Hatziargyriou, D. Hill, A. Stankovic, C. Taylor, T. Van

Cutsem, and V. Vittal, "Definition and classification of power system stability," *IEEE Trans. Power Syst.*, vol. 19, no. 2, pp. 1387–1401, May 2004.

[2] K. Kawabe and K. Tanaka, "Impact of dynamic behavior of photovoltaic power generation systems on short-term voltage stability," *IEEE Trans. Power Syst.*, vol. 30, no. 6, pp. 3416–3424, Nov. 2015.

[3] A. E. Hammad and M. Z. El-Sadek, "Prevention of transient voltage instabilities due to induction motor loads by static VAR compensators," *IEEE Trans. Power Syst.*, vol. 4, no. 3, pp. 1182–1190, Aug. 1989.

[4] Y. Sekine and H. Ohtsuki, "Cascaded voltage collapse," *IEEE Trans. Power Syst.*, vol. 5, no. 1, pp. 250–256, Feb. 1990.

[5] H. Ohtsuki, A. Yokoyama, and Y. Sekine, "Transient P-V curves used for analysis of transient voltage stability," in *Proc.* 10th-PSCC, Graz, 1990, pp. 1202–1209.

[6] C. D. Vournas and G. A. Manos, "Modelling of stalling motors during voltage stability studies," *IEEE Trans. Power Syst.*, vol. 13, no. 3, pp. 775–781, Aug. 1998.

[7] Z. Wang, X. Wang, and C. Y. Chung, "An analytical method for calculating critical voltage sag clearance time of induction motors," *IEEE Trans. Power Del.*, vol. 27, no. 4, pp. 2412–2414, Oct. 2012.

[8] K. Kawabe and K. Tanaka, "Analytical method for short-term voltage stability using the stability boundary in the P−V plane," *IEEE Trans. Power Syst.*, vol. 30, no. 6, pp. 30410–3047, Nov. 2014.

[9] NERC Transmission Issues Subcommittee and System Protection and Control Subcommittee, "A technical reference paper fault-induced delayed voltage recovery –Version 1.2," NERC, Atlanta, GA, 2009.

[10] Western Electricity Coordinating Council Modeling and Validation Work Group, "Composite load model for dynamic simulations," WECC, Salt Lake, UT, Rep. *1.0*, 2012.

[11] K. Fujii, N. Kanao, T. Yamada, and Y. Okuma "Fault ride through capability for solar inverters," in *Proc. 2011-14th European Conference on Power Electronics and Applications (EPE 2011)*, Aug. 30– Sept. 1, 2011.

[12] R. Yan and T. K. Saha, "Investigation of voltage stability for residential customers due to high photovoltaic penetrations," *IEEE Trans. Power Syst.*, vol. 27, no. 2, pp. 651–662, May 2012.

[13] M. S. E. Moursi, H. H. Zeineldin, J. L. Kirtley, Jr., and K. Alobeidli, "A dynamic master/slave reactive power-management scheme for smart grids with distributed generation," *IEEE Trans. Power Delivery.*, vol. 29, no. 3, pp. 1157–1167, Jun. 2014.

[14] R. K. Varma, S. A. Rahman, and T. Vanderheide, "New control of PV solar farm as STATCOM (PV-STATCOM) for increasing grid power transmission limits during night and day," *IEEE Trans. Power Delivery.*, vol. 30, no. 2, pp. 755–763, Apr. 2015.

[15] H. D. Tafti, A. I. Maswood, Z. Lim, G. H. P. Ooi, and P. H. Raj, "A review of active/reactive power control strategies for PV power plants under unbalanced grid faults," in *Proc. of Smart Grid Technologies (ISGT ASIA)*, Nov. 3–6, 2015

[16] WECC Renewable Energy Modeling Task Force. (2012, Sep.). Generic solar photovoltaic system dynamic simulation model specification, Power World Corporation, Illinois, U.S., [Online]. Available: http://www.powerworld.com/files/WECC-Solar-PV-Dynamic-Model-Specification-September-2012.pdf

[17] H. Kobayashi, "Fault ride through requirements and measures of distributed PV systems in Japan," in *Proc. IEEE Power Eng. Soc. General Meeting*, Jul. 22–26, 2012.

[18] H. Ohtsuki, A. Yokoyama, and Y. Sekine, "Transient P-V curves used for analysis of transient voltage stability," in *Proc.* 10th-PSCC, Graz, 1990, pp. 1202–1209.

K. Kawabe (M'12) received the B.S. degree from Waseda University, Tokyo, Japan, in 2007, and the M.S. and Ph.D. degrees from The University of Tokyo, Japan, in 2009 and 2012, respectively. He was a Visiting Assistant Professor with University of Toyama, Japan, from 2012 to 2016. He has been with the Department of Electrical and Electronic Engineering, Tokyo Institute of Technology, Japan, since 2016 as an Assistant Professor.

Y. Ota (M'04) received the B.S., M.S., and Ph.D. Eng. degrees from Nagoya Institute of Technology, Japan, in 1998, 2000, and 2003, respectively. He was a Project Assistant Professor with The University of Tokyo, Japan. He is currently an Associate Professor with Tokyo City University, Japan.

A. Yokoyama (M'78) received the B.Eng., M.Eng., and Dr. Eng. degrees from The University of Tokyo, Japan, in 1979, 1981, and 1984, respectively. He has been with the Department of Electrical Engineering and Information Systems, The University of Tokyo, since 1984 and is currently a Professor in charge of Power Systems Engineering. He was a visiting Research Fellow with the University of Texas, Arlington and the University of California, Berkeley, U.S. from 1987 to 1989.

K. Tanaka received the B.S., M.S., and Ph.D. degrees in Engineering from the Graduate School of Kyushu University, Fukuoka, Japan, in 1974, 1976, and 1996, respectively. He joined the Central Research Institute of Electric Power Industry in 1976 and served as a visiting Researcher with the University of Texas, Arlington, U.S. from 1981 to 1982. He has been a visiting Professor with the Graduate School of Science and Engineering, University of Toyama, Japan, since 2012.